2. SCANNING NEAR-FIELD OPTICAL MICROSCOPY IN NANOSCIENCES

ALEXANDRE BOUHELIER, ACHIM HARTSCHUH, AND LUKAS NOVOTNY

1. SCANNING NEAR-FIELD OPTICAL MICROSCOPY AND NANOTECHNOLOGY

The skills of Swiss watchmakers a couple of centuries ago started a trend of miniaturization aiming at controlling the material world on increasingly smaller scales. This trend never stopped ever since. The emerging field of nanoscience is leading to unprecedented understanding and control over the fundamental building blocks of matter. What was a playpen for physicists, chemists, and biologists, is rapidly evolving to mature technology and engineering. The possibility of artificially synthesized nanodevices that could become the basis for completely new technologies is the main driving force of today's investors. The way individual units organize into nanoscale patterns determines important material functionalities, including electrical conductivity, mechanical strength, chemical specificity, and optical properties. To map out the landscape of this nanoscale territory, new characterization tools have to be developed. The family of scanning probe microscopes offered scientists to zoom in on previously hidden nanoscale features. While the nanometric stylus of a scanning tunneling microscope travels over a sample surface like a blind's person stick, much could be learn if this stick was equipped with a "nano-eye", which optically look at the surface.

Extending optical perception to increasingly finer scales permitted early scientists to discover natural laws otherwise invisible. Over nearly 4 centuries, the basic design of a microscope did not really change conceptually. The legacy of Van Leeuwenhoek and Hooke is still a prime scientific tool. With the improvement of lenses in the 18^{th} and 19^{th} centuries, especially the effort done to correct aberrations, microscopists rapidly

pushed the optical microscope to its fundamental limit: the maximum resolving power of a microscope is governed by diffraction of light. The image of a point source is not a point! This limitation, imposed by the very nature of light, was predicted by E. Abbe [1]. Lord Rayleigh in the 19th century expressed the resolution barrier in a very concise form known as the Rayleigh criterion [2]. In a visionary idea, E. H. Synge predicted in 1928 that the diffraction limit could be overcome by reducing the illuminating light source to a volume smaller than the wavelength [3]. By raster scanning this source in close proximity over a sample surface provides an image with lateral resolution better than the one imposed by the diffraction limit. The experimental realization of the forgotten idea was independently achieved in Switzerland [4] and in the U.S [5] in the early eighties, soon after the discovery of the scanning tunneling microscope. Scanning near-field optical microscopy (SNOM or NSOM) was born and adds its name to the growing family of scanning probe microscopes.

Optics provides a wealth of information not accessible to other proximal techniques. The photon, as an observable, can reveal the identity of molecules, their chemical, material, and electronic specificity. Scanning near-field optical microscopy provides the "nano-eye" in the form of a nanometric light source confined at the end of a tip. An obvious advantage of the technique over many others is its versatility. The method has been successfully used in various environmental conditions, including low temperature, high vacuum, and in liquids depending on sample requirements. There are no fundamental restrictions on the object under investigation either. The sample can be transparent or opaque, flat or corrugated, organic or semiconductor. . .

Although technical issues rather than fundamental limits prevented near-field optics to advance to arbitrary high resolution, recent advances in nanofabrication and a better understanding of optical interactions on the nanoscale will potentially enable SNOM to be a prime characterization tool, in the same way as optical microscopy in the past centuries.

2. BASIC CONCEPTS

The angular representation of the field in a plane $z = z_0$ near an arbitrary object can be written as:

$$E(x, y, z_0) = \iint A(k_x, k_y) \exp i \left(k_x x + k_y y + z_0 \sqrt{\left(k_0^2 - k_x^2 - k_y^2\right)} \right) dk_x \, dk_y, \qquad (1)$$

where $A(k_x, k_y)$ represents the complex amplitude of the field, and $k_0 = \omega/c$ is the vacuum wave vector. Equation (1) is basically the sum of plane waves and evanescent waves propagating in different spatial directions. Wave vectors k_x and k_y smaller than k_0 constitute homogenous plane waves that propagate in free space. Wave vectors satisfying this condition have low spatial frequencies. Typically, a lens of a microscope collects wave vectors that are confined to $[0..k_{max} = n\omega \sin\theta/c]$, where θ is the semi-aperture angle of the lens and n is the refractive index. In terms of resolution, the distance Δx

between two point-like objects that can just be resolved with a conventional optical microscope using coherent illumination is given by:

$$\Delta x = 0.82 \frac{\lambda_0}{n \sin \theta}, \tag{2}$$

where λ_0 is the illumination wavelength in vacuum. This equation, derived from Abbe's theory, represents the theoretical resolution given by the diffraction of light. According to Eq. (2), the separation Δx can be decreased by using shorter illumination wavelengths (UV microscopy), and/or by increasing the index of refraction (oil or water immersion objectives, solid immersion lenses) and/or by increasing the collection angle θ.

The integration in Eq. 1 runs also over k_x and k_y values that are larger than ω/c. Consequently, the field components become evanescent. The electric field of evanescenet waves propagates in the x, y plane but is exponentially attenuated in the z-direction. These fields, associated with high spatial frequencies (fine details of an object), are not detected by the objective of a classical microscope. In order to achieve superresolution, the variations of the field in the immediate vicinity of the object have to be collected. The collection of evanescent waves is the basis of scanning near-field optical microscopy.

Evanescent waves can be converted to propagating radiation by local scattering. The smaller the scatterer is and the closer it is placed near the surface of an object, the better the conversion will be. According to Babinet's principle, local scattering is analogous to local illumination. This means that the small details of an object can be accessed by either scattering the evanescent fields created by the object with a small scattering center or by illuminating the object with evanescent fields created by a local source. The field produced by the local source is converted into farfield components by the minute dimensions of the object. The combination of the reciprocity theorem and Babinet's principle is at the origin of numerous possible arrangements used in near-field optical microscopy. Although they are phenomenologically different, they are conceptually identical and lead to similar results. The choice of one arrangement over another is mainly driven by the optical characteristics of the sample. A more detailed description of common configurations will be described later.

3. INSTRUMENTATION

Scanning near-field optical microscopy belongs to the family of proximal probe microscopy such as scanning tunneling (STM) and atomic force microscopy (AFM). In these techniques, high resolution is achieved by minimizing the interaction volume between a probe and an object. The probe takes form of a tip where only the very apex is responsible for the interaction. Similarly, near-field optics uses a small probe to confine an optical interaction between probe and sample. Control over probe manufacturing is a prerequisite for routine high-resolution imaging. Unlike the successful batch microfabrication of AFM cantilevers, the fabrication of near-field probes is the

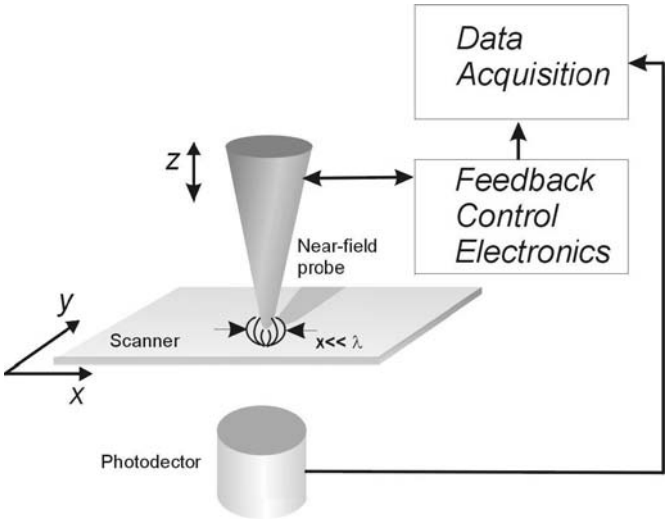

Figure 1. Schematic of a near-field optical microscope. A near-field probe confines an optical interaction to dimensions much smaller than the wavelength. A photodector collects the optical response for each probe position. The signal is read by an acquisition module, which reconstructs a two-dimensional optical image of the surface. A feedback system controls the distance between probe and sample surface to a few nanometers. Finally, a scanning stage translates the sample (or the tip) in a lateral direction.

Achille's heel of SNOM. A discussion of the role of nanotechnology in probe manufacturing will be reviewed in the next section.

The basic units forming a near-field microscope are very similar to an AFM or a STM. As depicted in Figure 1, it consists of (i) a near-field probe confining an optical interaction to dimensions smaller than the wavelength, (ii) a scanning stage permitting to move the sample or the tip laterally, (iii) a photodetector to collect the response of the optical probe-sample interactions, and finally (iv) an acquisition software to reconstruct an optical image. SNOM specifications require that the tip sample distance should be controlled with sub-nanometer precision and shear-force regulation [6] based on quartz tuning fork is extensively used [7]. The damping of a laterally oscillating tip caused by the mechanical interactions with the surface (shear forces) depends on the tip-sample separation. This damping signal is fed to a feedback mechanism (v), which controls the distance between tip and sample via a piezoelectric actuator (not shown).

3.1. Probe Fabrication

In order to retrieve the high spatial frequencies of an object, a probe is brought in close proximity of the object's surface. An image is reconstructed by scanning the probe in the plane of the sample. The lateral resolution in a near-field optical image is determined, to first approximation, by the size of the optical probe. However, the

fabrication of optical probes with sub-wavelength dimensions is technically challenging, and nanotechnology plays an important role in the fabrication processes.

3.1.1. Optical Fiber Probes

Sharply pointed optical fibers are widely employed in scanning near-field optical microscopy. These probes can be used as local scatterers or as nanosources. Optical fibers have the advantage of low fabrication costs and low propagation losses. The guiding properties of these waveguides fulfill the conditions needed for near-field applications to a large extent. Polarization for instance, can be accurately controlled in the fiber. It finds important applications for the interpretation of contrast [8]. Furthermore, the operation wavelength of fibers spans from the visible to telecom wavelengths, which can be useful for recording spectroscopic information.

The central step in probe manufacturing is the formation of a taper region to form a nanometric glass tip terminating one end of the fiber. Two methods are usually employed. One approach, the so-called pulling technique, is adopted from microbiology where it is used to produce micropipettes. A pulled fiber is obtained by locally melting the glass with the help of a CO_2 laser or a hot coil. Springs attached to both ends pull the fiber apart resulting in two tapered ends [9]. In elaborate commercially available puller, parameters such as heating time, pulling force or delay time can be adjusted to control the shape of the taper. The surface of the taper is usually very smooth as a result of the local melting during the pulling process. The end of the fiber is commonly terminated by a plateau, which can vary in size depending on the pulling parameters. Alternatively, glass is a material that can be etched by chemicals such as hydrofluoric acid (HF). A bare glass fiber (without the protective polymer jacket) is dipped into a bath of HF. The surface tension of the liquid forms a meniscus at the interface between air, glass, and HF. A taper is formed due to the variation of the contact angle at the meniscus while the fiber is etched and its diameter decreases [10]. The surface tension can be modified by the addition of surface layer atop the HF. As a result, the cone angle of the taper can be slightly varied. This function is more difficult to control with the pulling technique. A striking difference, as compared to a pulled fiber is the surface roughness of the taper. The acid leads to irregular surfaces because of inhomogeneities in the glass and because of the sensitivity of the technique to outside perturbations (temperature, vibrations . . .). Alternative etching techniques have been developed to improve the surface roughness. Among them, is the tube-etching technique [11, 12] or buffered HF solutions [13] that tend to reduce the influence of external perturbations. A comparison between mechanically pulled and chemically etched fibers is provided in Refs [14, 15]. Without going into details, pulled fibers have small cone angles which are not favorable for high throughput [16] and have a flat end face that somewhat limits the size of the tip. On the other hand, their smooth surface benefits the deposition of homogeneous metal coatings as discussed later. Etched fibers have a rough surface caused by the acid attack. Consequently, the quality of a deposited metal coating is not as good. The main advantage of etching is that the cone angle of

the taper can be varied and the transmission of metal-coated probes can be drastically improved [16].

3.1.2. Aperture Formation

The guiding properties of an optical fiber are well understood [17]. In the taper region, a propagating mode becomes increasingly delocalized, *i.e.,* the field reaches out of the fiber core [18, 19]. The consequence is that while the extremity of the fiber can be a few tens of a nanometer, the spatial extension of the mode exceeds this dimension by far. To confine the mode and to guide it to the very tip, a metal coating is deposited on the outside surface of the fiber. The layer acts as a reflector and therefore prevents the light to spread out of the fiber. Aluminum, silver and gold are the most commonly used materials owing to their good optical properties at visible wavelengths (small skin depth and high reflectivity). If the metal coating covers the entire taper region, the fiber will be opaque and no light will be transmitted or collected. For the light to escape, a sub-wavelength hole-or aperture-is needed at the very apex of the coated tip. The fabrication of such an aperture with nanometer sized dimensions poses a variety of technical difficulties. These are discussed in the next sections.

A) SQUEEZING TECHNIQUE In the early work of D. W. Pohl *et al.*, a completely metal-coated optical waveguide was squeezed towards a hard surface in order to press the metal away from the foremost end. Applying an offset voltage on an extendable piezoelectric tube can control the pressure on the tip. Cold deformation and abrasion take place at the end of the tip eventually forming a tiny aperture [4]. Monitoring the light throughput of the tip controls the formation of the aperture. The obtained apertures are fairly small (∼80 nm) and the end faces are flat. This technique provided high-resolution images on individual fluorophores [20] and seems to regain some attention recently.

B) SHADOWING TECHNIQUE The most widespread technique to produce a small aperture uses the so-called shadowed evaporation scheme. In this approach, the apertures are produced at the time of metallization in an evaporation chamber. A metal coating is deposited such that the very apex of a fiber tip is left uncoated. This is accomplished by evaporating the metal in a direction slightly inclined to the tip axis. A homogeneous film thickness is deposited around the fiber by rotating the fiber during the evaporation process. This method is well suited for the fabrication of apertures of many tips at once. Unfortunately, the aperture shape and diameter are not reproducible between successive evaporations or even between tips evaporated at the same time. The main reason of the poor reproducibility is the number of parameters involved: tilt angle, distance to the source, rotation speed, evaporation rate, base pressure and film thickness. Furthermore, the intrinsic roughness of the metal surface also influences the quality of the apertures. An example is shown in Figure 2(a) where an electron microscope was used to image the end face of a tip. The aluminum layer is readily seen in the image. It is surrounding a dark center representing the physical aperture. An aluminum grain is obscuring part of the opening leading to an asymmetric aperture.

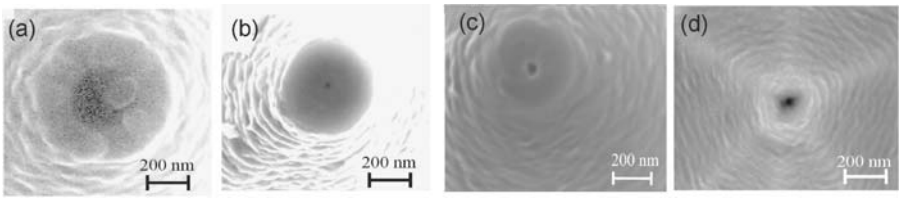

Figure 2. Gallery of apertures produced with different approaches listed in the text. (a) Shadowing technique. Courtesy of B. Hecht, University of Basel. (b) Electroerosion. (c) Focused ion beam milling. Courtesy of Th. Huser, Lawrence Livermore National Laboratory. (d) Cantilever probe. Courtesy of L. Aeschimann and G. Schürmann, IMT Neuchâtel.

c) ELECTRO-EROSION The properties of solid amorphous electrolytes such as $AgPO_3$:AgI compounds provide a unique capability of material transport through a nanoscale area. It has been successfully demonstrated that the high ionic conductivity can be employed to remove the overcoating metal layer from the very apex of fiber tips [21, 22]. In this approach, a tiny electrolytic contact is formed between a tip that is entirely overcoated with metal and the surface of the electrolyte. A bias voltage triggers the erosion of the metal layer. A feedback mechanism is used to keep the ionic current constant, thereby controlling the metal removal rate from the tip. Similar to the squezzing technique, aperture formation is monitored by collecting the light transmitted through the tip. Near-field apertures with diameters below 50 nm can be manufactured by electro-erosion (see Figure 2(b)).

d) FOCUSED ION BEAM MILLING Focused ion beam (FIB) milling is a technique that uses a beam of accelerated ions to modify materials with nanometer precision. In standard instruments, a Gallium source is ionized and the emitted ions are focused into a spot of a few nanometers on the surface of the sample. The energy of the ions is sufficient to ablate material from the sample surface. In the context of aperture formation, the ion source is directed at the apex of a pre-coated tip at an angle of 90° to the tip axis. The end of the tip is sliced away such that the slicing beam cuts through the metal coating as well as the fiber core [23, 24]. The aperture definition, the flatness of the tip end face, the polarization behavior and the imaging capabilities of such processed probes make them suitable for high resolution imaging as demonstrated by investigations of single fluorescent molecules [24]. A scanning electron micrograph of the end face of a FIB-fabricated aperture is shown in Figure 2(c). Although, this approach seems to overcome most of the problems associated with aperture fabrication, the instrument cost is considerable.

e) OTHERS METHODS A plethora of alternative techniques has been used with varying success. Among them is the so-called triangular probe or T-probe. The triangular shape originates from a tetrahedral hollow waveguide coated with an aluminum layer and squeezed against a hard surface to produce an aperture [25]. Another interesting concept described by Fischer and Zapletal was introduced to potentially overcome

some of the limitations of aperture-based near-field probes [26]. The authors suggested the use of a coaxial tip as a SNOM probe. In theory, a coaxial waveguide is able to focus electromagnetic fields down to a spot much smaller than the wavelength without any cutoff of propagating modes. Despite the suitability of such optical properties, technical difficulties are still limiting the fabrication of coaxial probes.

3.1.3. Cantilever Probes

Recently, a new probe concept was introduced that is based on a micro-machined tip. It makes use of technology developed for atomic force microscopy (AFM), which is well established in various fields of science. The interaction between probe and sample is well understood, making AFM a rather easy to operate instrument even for non-specialists. AFM probes are batch fabricated which reduces the cost of fabrication. In order to be useful for optical applications, a cantilever has to be transparent for the light to pass. Silicon nitride or quartz is usually the chosen material. While the tips can be made using standard micromachining techniques, cantilever-based optical probes face the same difficulties as those associated with optical fiber based probes. Two main approaches are applied for the fabrication of AFM probe apertures: reactive ion etching [27] and direct-write electron beam lithography [28]. Figure 2(d) shows a scanning electron micrograph of a cantilever tip. Recently, a self-terminated corrosion process of the aluminum film was applied to produce successfully sub-50 nm apertures [29].

3.1.4. Metal Tips

So far, we considered probes that act as optical waveguides, i.e. they guide light to or from a nanoscale area. A second class of optical probes utilizes bare metal tips as used in STM. The technique is referred to as apertureless scanning near-field optical microscopy. A metal tip, usually tungsten, locally perturbs the electromagnetic field surrounding the specimen. The locally scattered information is discriminated from the unavoidable farfield scattered signal with lock-in and demodulation techniques. This scattering approach demonstrated material specificity with outstanding resolution both in the infrared and the visible region [30].

Alternatively, one can benefit from the strong enhancement of the electric field created close to a sharply pointed metal tip under laser illumination. This phenomenon originates from a combination of surface plasmon resonances and an electrostatic lightening rod effect [31]. The energy density close to the metal tip can be orders of magnitude larger than the energy density of the illuminating laser light. This enhancement effect is mainly used to increase the response of spectroscopic interactions such as fluorescence or Raman scattering. Examples of such applications are discussed in section 4. More recently, some experimental and theoretical research was directed at the combination of fiber-based near-field probes with field enhancing metal tips [32, 33]. Preliminary results showed lateral resolutions better than 30 nm. The main advantage of this combination is the reduction of the excitation area as well as the absence of alignment procedures between tip and laser beam.

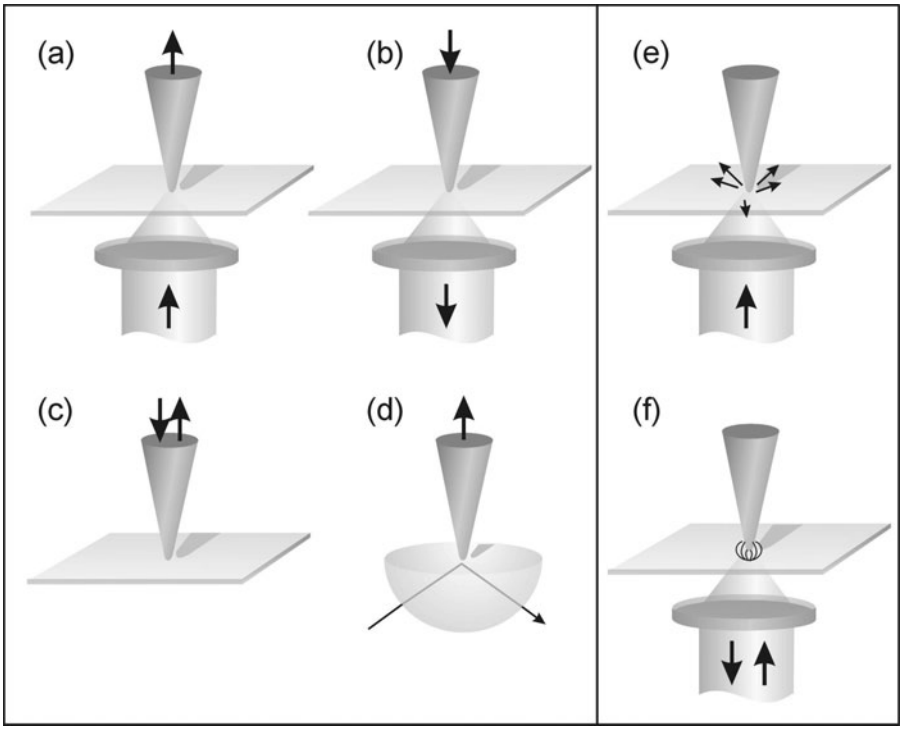

Figure 3. Schematic of the most common SNOM configurations. (a–d) aperture-based probes. (a) Farfield illumination and local probing of the near-field. (b) Near-field illumination, and farfield collection. (c) Local illumination and collection. (d) Dark field illumination. (e–f) Metal tips. (e) Farfield illumination and local scattering at the tip. (f) Local field enhancement created by farfield illumination.

3.2. Flexibility of Near-Field Measurements

As discussed in the previous section, there is no fundamental difference between locally illuminating an object and locally probing the field near it. The essence is that the confinement of the photon flux between probe and sample defines the optical resolution. In turn, many experimental variations can be employed to locally create a confined optical interaction and, for a non-specialist, the literature can be quite confusing.

Figure 3 depicts the most common configurations, emphasizing the flexibility of the technique. Near-field instruments are usually separated into two categories depending on the type of probe used: aperture-based (optical fiber, AFM cantilever) or metal-based (scattering and field enhancement). Sketches (a–d) represent configurations where a nano-aperture is used either as a nanocollector or as a local source. In Figure 3(a), an object is illuminated from the farfield using standard optics. An aperture-based tip is placed close to the surface to collect the near-field. Figure 3(b) depicts the opposite situation. The aperture now illuminates the specimen, and the response is collected with conventional farfield optics. These two configurations are commonly used for thin

transparent samples due to the fact that the signals are *transmitted* through the object. However, alternative farfield illumination\collection systems can be implemented from the side to overcome some of the sample restrictions. Figure 3(c) represents a combination of the two previous configurations. Illumination and collection are both performed locally in the near-field of an object. The last configuration based on aperture probes is shown in Figure 3(e). The design can be viewed as the near-field analogue of a dark-field microscope. Illuminating the object with evanescent waves created by total internal reflection (TIR) drastically reduces the background farfield light. The technique emphasizes the fact that a near-field probe *frustrates* the evanescent field [34]. This configuration is widely used for the imaging of non-radiative electromagnetic fields. Applications range from waveguide characterization to imaging of planar plasmonic and photonic structures as discussed in the next section.

The second class of near-field microscope is depicted in Figure 3(e–f). Here, the aperture is replaced by a metal tip, which performs two functions, scattering and/or enhancing a near-field signal, depending on tip material and illumination conditions. In the first example, Figure 3(e), a tip locally scatters the near-field of an object that is illuminated by farfield means. The locally scattered signal is collected also by conventional optics. The illumination, here performed from the bottom of the object, can be implemented from the side of the tip. The choice between one illumination scheme and another is mainly governed by sample requirements. Finally, Figure 3(f) schematically represents a metal tip used as a signal enhancer. Favorable illumination of the tip creates an enhanced field at the tip end that is used as a local light source. The increased sample response is usually collected with the same optics used to illuminate the tip.

4. APPLICATIONS IN NANOSCIENCE

The trend toward nanoscience and nanotechnology is mainly motivated by the fact that the underlying physical laws change from macroscopic to microscopic. As we move to smaller and smaller length scales, new characterization techniques have to be developed to probe the properties of novel nanostructures. There is a continuing demand for new measurement methods that will be positioned to meet emerging measurement challenges.

4.1. Fluorescence Microscopy

Optical spectroscopy provides a wealth of information on structural and dynamical characteristics of materials [35]. Combining optical spectroscopy with near-field optical microscopy is especially desirable because spectral information can be spatially resolved. The need for improved spatial resolution currently limits the ability of industry to answer key questions regarding the chemical composition of surfaces and interfaces.

The detection and manipulation of a single molecule represents the ultimate level of sensitivity in the analysis and control of matter. Measurements made on an individual molecule are inherently free from the statistical averaging associated with conventional

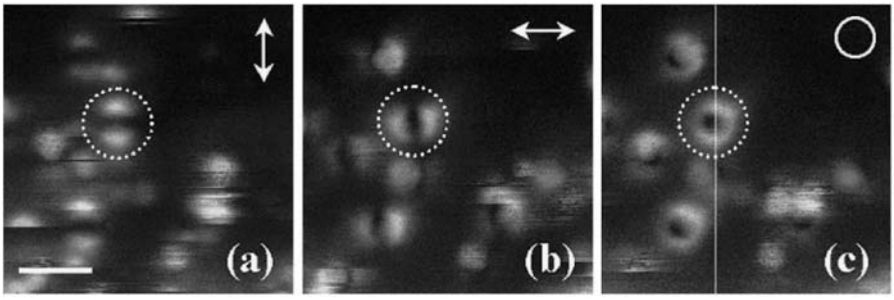

Figure 4. Series of three successive SNOM fluorescence images of the same area (1.2 by 1.2 μm) of a sample of $DiIC_{18}$ molecules embedded in a 10-nm thin film of PMMA. The excitation polarization (as measured in the farfield) was rotated from one linear polarization direction (a) to another (b) and then changed to circulat polarization (c). The fluorescence rate images of the molecules change accordingly. The molecule inside the dotted circle as a dipole axis perpendicular to the sample plane. Scale bar: 300 nm. From Ref. [24].

ensemble experiments. Single molecule techniques have a diverse range of existing applications in physics, chemistry, and biology [36]. Potential applications include single photon sources for quantum computing and massively parallel DNA sequencing. Furthermore, the local environment influences the molecular properties of species and monitoring the behavior of the fluorescence provides a sensitive probe for the molecule's local environment.

The potential of scanning near-field optical microscopy for imaging molecular systems has been recognized by two groups in 1986 [37, 38]. However, the first observation of single molecules using optical near-field technique came 7 years later [39]. In this pioneering experiment, single carbocyanine $DiIC_{12}$ dye molecules were embedded in a polymer matrix and dispersed on a glass substrate. A near-field probe made from an aluminum-coated glass fiber optically excited the molecules. The probe was raster scanned over the sample plane. The fluorescence of individual molecules was collected by a large numerical aperture objective to ensure high collection efficiency. In this remarkable paper, the authors could determine the orientation of the absorption dipole moment of each molecule by recording the spatial variation of the fluorescence as the aperture moved over the molecules. A molecule is excited only if a component of the optical electric field is polarized along its transition dipole moment. Because of the laterally and longitudinally polarized electric fields near the aperture of the probe, randomly oriented molecules can be efficiently excited. Emission patterns of single molecules turned out to be sensitive probes for the electromagnetic field distribution near a near-field probe and be suitable for the determination of molecular orientations. Veerman *et al.* have published a systematic study of this effect [24]. Figure 4 represents a series of near-field images of individual emitters for three consecutive excitation polarizations. Each pixel of the images represents the fluorescence rate for a particular tip position. By changing the polarization state of the near-field excitation, the orientation of the dipole moment can be fully determined.

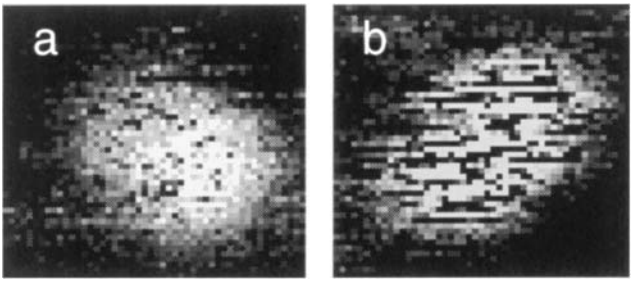

Figure 5. (a) and (b): Near-field fluorescence image of two different single DilC18 molecules embedded in a 10 nm PMMA layer (370 by 370 nm). Dark pixels are due to temporal quantum jumps to the first excited triplet state. From Ref. [44].

Because of the dependence of a molecule's fluorescence on the local environment, the molecule's properties are influenced by the proximity of an aluminum-coated fiber tip. The fluorescence lifetime was found to be dependent on the relative position between a molecule and the near-field probe [40]. Furthermore, the radiation pattern of a dipole can be modified by the presence of a near-field tip; much alike a dipole radiation pattern is distorted by the presence of a nearby interface [41]. It was found that the radiation pattern for in-plane oriented molecules are distorted in the direction of the center of the near-field aperture while for out-of-plane oriented molecules the distortion is in the direction of the metal coating covering the glass fiber tip [42].

Measurements on individual molecules on a nanometer scale give unique insight on their complex dynamic behavior. Photobleaching of single emitters was observed for the first time, revealing on and off state of the molecule before its final and irreversible photochemical modification [43]. Time-resolved investigations attributed the dynamics of the instable molecular emission to the occupation of the lowest excited triplet state. As long as this state remains populated, the fluorescence is interrupted momentarily leading to a photon-bunching effect as seen in Figure 5 [44]. The lifetime of the triplet state is intimately linked to the environment of the molecule providing thereby a local probe for the nanoenvironment. An interesting side note is that these measurements satisfy the ergodic principle: the same triplet state lifetime distribution is measured on a single molecule at different instants in time and for a set of molecules at the same instant in time.

Near-field optical fluorescence microscopy is successfully used to investigate more complex systems than single molecules. In particular, SNOM is a promising method to study biological systems where resolution is an important parameter. An example of such biological system is nuclear pore complexes (NPCs). Single NPCs cannot be images with conventional microscopy due to the fact the nearest neighbor distance is in the range of 120 nm. The high lateral optical resolution of SNOM can provide detailed insight into the transport dynamics of a single NPC [45].

The lateral resolution obtained with optical near-field techniques is, to a good approximation, given by the diameter of the sub-wavelength aperture. Fluorescence

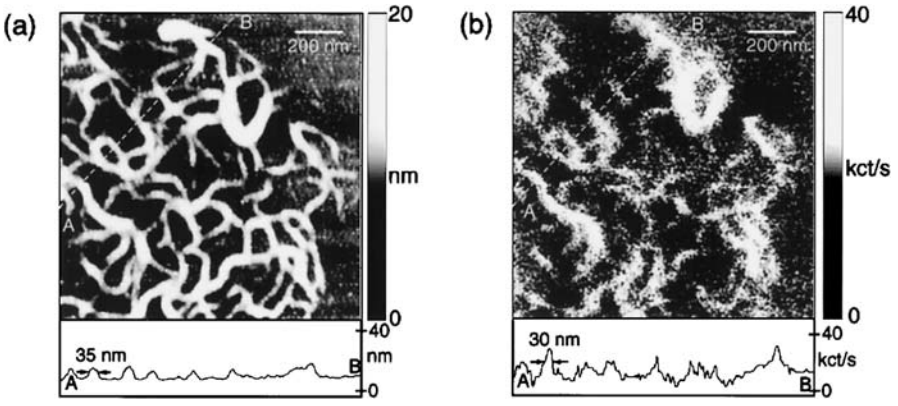

Figure 6. Simultaneous topographic image (a) and near-field two-photon excited fluorescence image (b) of *J*-aggregates of PIC dye in a PVS film on a glass substrate. The topographic cross section along the dashed line (A–B) has a particular feature of 35-nm FWHM (indicated by arrows) and a corresponding 30-nm FWHM in the fluorescence emission cross section. From Ref. [49].

images with 15 nm resolution have been reported [46]. However, there are two fundamental limits preventing higher resolutions. The first one is the penetration of light into the metal coating surrounding the aperture. The skin depth defines the ultimate excitation volume of an aperture, and aluminum is the best coating choice in the visible region. A second limitation is the throughput of a nanometer-sized aperture. The farfield transmission of a sub-wavelength aperture inversely scales with the sixth power of the radius [47]. For a small aperture, the signal-to-noise ratio becomes an important factor in the contrast formation of an image and alternative techniques might be necessary. One way to overcome the signal-to-noise limitation is to increase the fluorescence yield of individual molecules through a local field enhancement effect.

Metal nanostructures are successfully used to enhance the response of particularly small scattering and fluorescence cross-sections [48]. A metal tip can strongly enhance the electric field at its apex through a combination of an electrostatic rod effect and surface plasmon resonances [31]. If the tip is held over a fluorescent sample, the emission yield can be enhanced manifold. This technique was successfully applied to photosynthetic membranes and molecular aggregates, revealing spectroscopic information with a spatial resolution less than 30 nm [49] as shown in Figure 6.

Another promising mechanism that could potentially increase the resolution of a near-field microscope further is the so-called fluorescence resonance energy transfer (FRET) technique. FRET occurs on intermolecular distances of 1 to 8 nm. The energy from a donor molecule can be transferred nonradiatively to an acceptor molecule. The transfer efficiency depends on the inverse sixth-power of the distance between donor and acceptor and on their spectral overlap. This sensitivity can be used to further extend the fluorescence imaging capability of SNOM. Single pair FRET was demonstrated on DNA-linked donor-acceptor where the excitation of the donor was performed by

a near-field probe [50]. Development towards true molecular resolution involves the combination of a functionalized tip, where donor (or acceptor) molecules have been attached, with an acceptor (or donor)-doped sample. The group of Dietler and Dunn carried out first attempts simultaneously [51, 52]. To date, the marriage of SNOM and FRET remains a technical challenge, mainly driven by the difficulties to functionalize the probing tips.

4.2. Raman Microscopy

Combined with near-field techniques, Raman spectroscopy is a promising tool for identifying and analyzing the molecular composition of complex materials. Vibrational spectra directly reflect the chemical composition and molecular structure of a sample. By raster scanning the sample and pointwise detection of the Raman spectra, chemical maps with nanoscale resolution can be obtained. A main drawback of Raman methods is the low scattering cross-section, typically 14 orders of magnitude smaller than those of fluorescence. Furthermore, the high spatial resolution achieved in near-field optics is linked to tiny detection volumes containing only a very limited number of Raman scatterers. The weakness of Raman signals in combination with the limited transmission of typical aperture probes [16] requires extended integration times even intermediate aperture sizes of about 150 nm [53, 54, 55]. An essential improvement of the spatial resolution below 50 nm with smaller apertures appears to be unfeasible.

A more promising approach makes use of the enhancement of the electric field in the proximity of nanometer sized metal structures known as surface enhanced Raman scattering (SERS). SERS is known since more than 20 years and enormous enhancement factors of up to 14 orders of magnitude have been reported allowing even for single molecule Raman measurements (see e.g. [48]). In these cases, a combination of different enhancement mechanisms is discussed. The strongest contribution is the electromagnetic enhancement caused by locally enhanced electric fields. An additional contribution results from a chemical effect that requires direct contact between scatterer and metal surface. By using a sharp metal tip, the enhancement effect can be confined to a very small volume at the end of the tip. This localized enhancement allows to selectively address different parts of the sample area and tip-enhanced spectroscopy of nanoscale sample areas can be achieved.

Tip-enhanced Raman spectroscopy has been used on a variety of different systems such as dyes and fullerene films, KTP crystals as well as single-walled carbon nanotubes (SWNT) [56, 57, 58, 59, 60] for a recent review see [61]. In this section, we review some of these studies to demonstrate the three key advantages of the method: high spatial resolution, signal enhancement (enhanced sensitivity), and chemical specificity.

High-resolution near-field Raman imaging of SWNTs on glass is demonstrated in Fig. 6. The Raman image (Fig. 6(a)) clearly shows the characteristic one-dimensional features of SWNTs, which are also seen in the simultaneously detected topographic image (Fig.6 (b)). In the topographic image however, additional circular features are present caused by water condensation. Importantly, these features are not observed in the Raman image demonstrating the chemical specificity of the method. The chemical

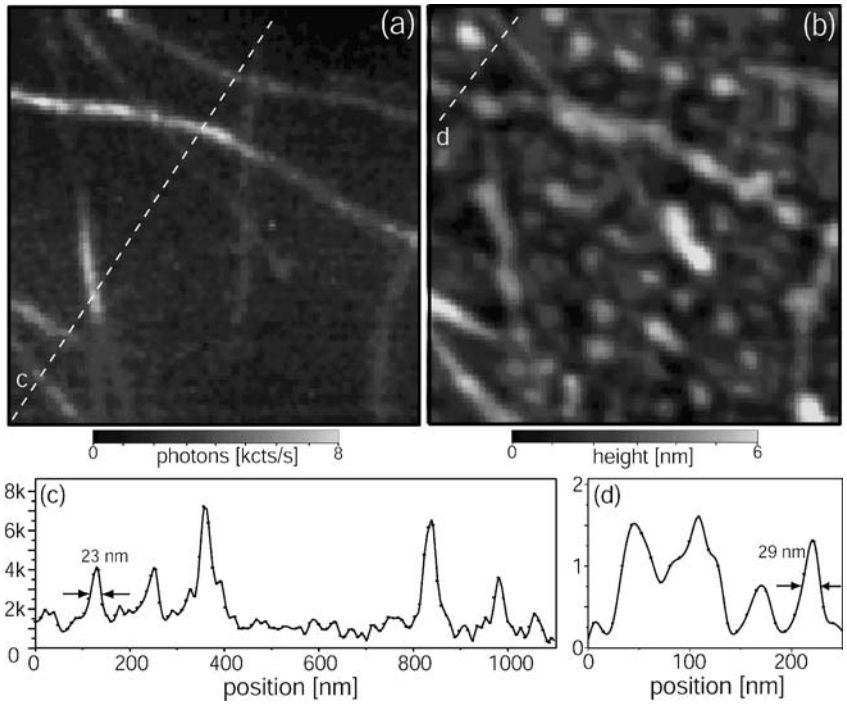

Figure 7. High spatial resolution near-field Raman image (a) and simultaneously detected topographic image (b) of single walled carbon nanotubes (SWNT) on glass. Scan area $1 \times 1\ \mu m^2$. The Raman image is acquired by detecting the intensity of the G′ band upon laser excitation at 633 nm. No Raman scattering is detected from humidity related circular features present in the topographic image indicating excellent chemical specificity (see text). (c) Cross section taken along the indicated dashed line in the Raman image. (d) Cross section taken along the indicated dashed line in the topographic image. The height of individual tubes is 1.4 nm. Vertical units are photon counts per second for (c) and nanometers for (d). From Ref [62].

specificity of the Raman scattering was also used to study local variations in the Raman spectra at the end of a SWNT [62]. In [57], spatial fluctuations within a mixture of dye molecules were investigated. In Fig. 6(c) and (d) cross-sections taken along the dotted lines in Fig. 6(a) and (b) are presented. The signal width (FWHM) observed in the Raman cross section (Fig. 6(c)) is about 23 nm, far below the diffraction limit of light used in the experiment.

The signal enhancement achieved in tip-enhanced Raman spectroscopy can be demonstrated by comparing the Raman spectra detected in presence and absence of the enhancing metal tip. In Fig. 7(a) and (b) examples for different organic molecules are shown. In order to determine the actual signal enhancement factors, the different sample volumes probed in either case have to be considered. The farfield spectrum detected without tip results from a diffraction limited area while the near-field spectrum with tip originates from the much smaller near-field area only. For a quantitative

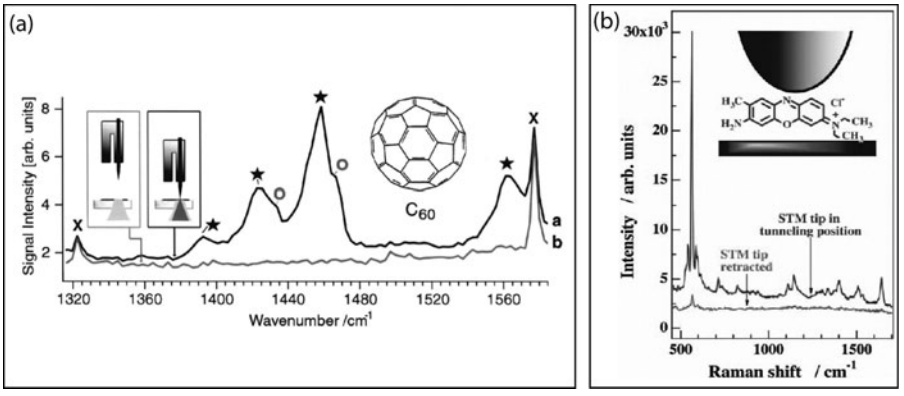

Figure 8. Signal enhancement achieved by tip enhanced Raman spectroscopy for a film of (a) C60 molecules on glass and (b) dye molecules (Brilliant Cresyl Blue) on top of a smooth gold film. From Ref. [56] [61].

discussion of the enhancement factors, these areas as well as the numbers of Raman scatterers therein have to be known. While this is difficult for dye films, the number of SWNTs can be determined based on their topography [62]. For the enhancement factors achieved, values ranging from 40 to 40000 have been reported by different groups. A listing can be found in [61].

An important question is whether the tip acts as a uniform amplifier of the complete Raman spectrum or whether the tip-enhancement varies for different Raman bands. Modifications of the relative strength of Raman lines could arise from different distributions of the filed polarization components in the near-field and farfield [59, 53]. In [63], new Raman signals are explained by significantly altered selection rules caused by the large field-gradients close to metallized aperture probes. Additional effects can also occur depending on the nature of the tip—sample distance control. In the case of AFM tapping mode and direct contact between tip and scatterer, additionally observed Raman bands have been attributed to chemical enhancement effects [56, 57]. For the larger distances of 1–2 nm (used in shear-force mode), no chemical enhancement is expected [62] while the possibility of sample material pick-up by the tip is reduced [61].

Raman methods are applicable to a large variety of systems since Raman scattering is an intrinsic property of all molecular structures. In contrast to fluorescence microscopy, there is no need for highly fluorescent samples or labeling with additional dye molecules. A further increase of the signal enhancement through optimization of the tip shape, tip material [64] and illumination mode [32] will open up fascinating insights into complex materials and might even enable for imaging of single biomolecules such as individual membrane proteins.

4.3. Plasmonic and Photonic Nanostructures

Nanoscale processes are physical interactions at the elementary level and their understanding is primordial for the design of nano-devices. The miniaturization of

optoelectronic circuits, for instance, is justified if the operating time can be made sufficiently short for fast computing. The combination of ultrafast and localized phenomena is therefore of considerable interest. In this regard, surface plasmons are very attractive: they can be well localized [65] and they exhibit ultrafast dynamics [66].

4.3.1. Surface Plasmon Polaritons

At optical frequencies, the electromagnetic properties of metals are far from being ideal. The concept of the electrons gas, however, is still valid and instrumental for the understanding of plasmon phenomena, *i.e.*, collective electron density oscillations. On metal surfaces or nano-structures a surface plasmon causes a variety of optical effects, among them strong local field enhancement and confinement of charge fluctuations at the interface [67]. Surface plasmons are a class of polaritons: a coupled matter-electromagnetic mode in which electromagnetic energy is carried by electrons that behave collectively. An interesting property of surface plasmons is that their mean free path, in the visible frequency range, can extend to several tens of micrometers while being strictly confined to the surface [68]. The non-radiative nature of surface plasmons and their long propagation length open the possibility to design planar structures for a variety of applications including biological sensors and miniaturized photonic circuits [69]. On a flat metal surface, surface plasmons cannot be excited with direct radiation. The momenta of surface plasmons are larger than the momentum of a free propagating photon of the same energy. However, light traveling in a higher index medium (e.g. glass) can transfer its energy to a surface wave and can be coupled to surface plasmon [70, 71]. Another technique that can provide the missing momentum is scattering of light by subwavelength structures [72] or holes [73] as discussed later.

Until recently, surface plasmons were detected by indirect means such as reflection measurements. Because of the non-radiative nature of surface plasmons one cannot rely on conventional imaging techniques to gain insights on their intrinsic properties. Fortunately, the development of optical near-field techniques and their capability to image evanescent fields triggered a rapid development of surface plasmon understanding.

In most studies, surface plasmons are excited by a laser beam that is reflected at a glass\metal\air interface (e.g. total internal reflection inside a prism). A dip in the angular reflection measurement indicates that the photon energy is coupled to a surface wave on the metal film. A near-field probe can be used to collect the near-field intensity associated with the plasmon. A spatial intensity map can be constructed by raster scanning the tip over the surface. An example is depicted in Figure 9. The authors compared two near-field intensity distributions. Figure 9(a) represents the near-field distribution created by a Gaussian beam that is totally reflected from a prism surface. Figure 9(b) pictures a surface plasmon intensity distribution excited on a thin silver film. The main difference resides in a tail in Figure 9(b) due to the surface plasmon propagation [74]. The same method was applied to the influence of surface corrugations on plasmon propagation [75]. It was shown that scattering by film imperfection causes non-negligible damping and thus a shortening of the plasmon mean free path [76].

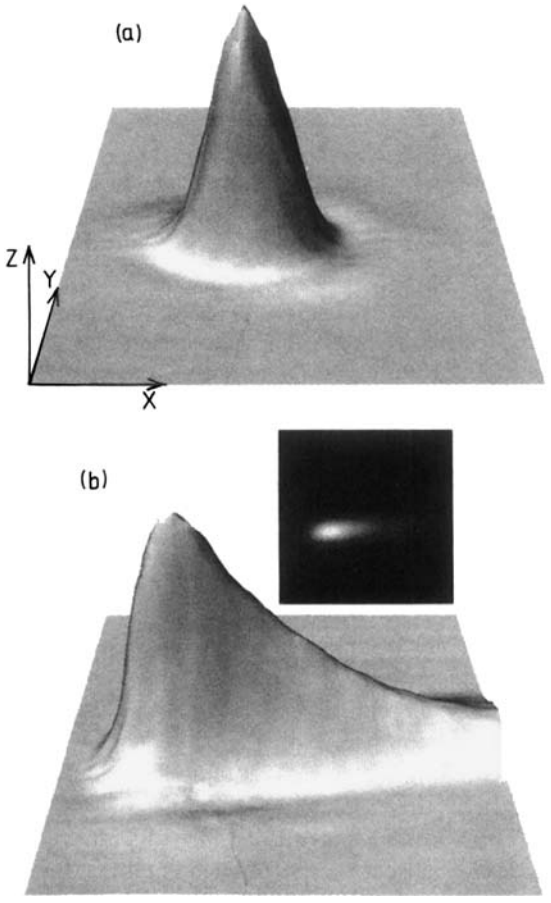

Figure 9. (a) Image of evanescent field intensity of a total internally reflected beam on prism surface. Scan range is 40 μm by 40 μm. (b) Image of the same field but with an additional 53 nm thick silver layer deposited atop the prism surface. The exponentially decaying tail is due to surface plasmon propagation. Inset: two-dimensional view of the image. From Ref. [74].

As already discussed above, the momentum mismatch between a free propagating photon and a surface plasmon can be overcome by diffracting a light beam through a subwavelength opening. The opening can take the form of holes in a thin silver film [77] or can be a near-field aperture located at the end of an optical fiber [78]. The field emitted by a sub-wavelength optical probe has a broad spatial spectrum. When such a probe is placed in close vicinity of a thin metal film, the large wave vectors ($k_{\|}$) fulfill the dispersion relation of surface plasmons and hence light can be coupled to a collective electron oscillation on the metal surface. The obvious advantage of this configuration is that surface plasmons are locally excited in a region of interest, e.g. next to nanostructures on the film surface. In many experimental configurations

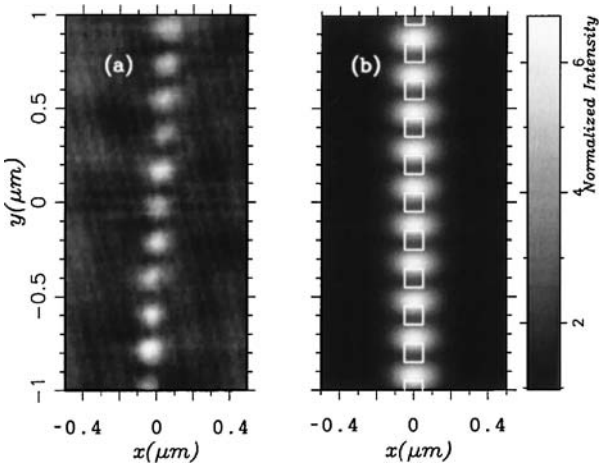

Figure 10. Image of the field distribution above a chain of Au particles (100 nm by 100 nm by 40 nm) acquired in collection mode. The field localization originated from particle-particle interactions. A comparison with a numerical simulation (b) shows that the bright spots are not on top of the Au particles (the surface projections of the particles correspond to the white squares). The intensity scale of experimental data (a) is normalized to the one of the numerical calculation (b). From Ref. [81].

the radiative decay surface plasmons can be imaged at any point in time [78, 79]. This approach permitted the quantitative evaluation of basic surface plasmon optical properties such as reflection and transmission coefficients [76, 80].

4.3.2. Plasmonic and Photonic Nanostructures

Surface plasmons are not only modes supported by thin metal films, but also by small metal particles where the cause peculiar optical phenomenon. Optical responses of individual particles are well understood and can be described accurately by Mie theory. The properties of mutually interacting particles are, however, of great current of interest, notably in the context of photonic crystals and biosensors. Photonic crystals have the unique ability to inhibit light propagation at certain wavelengths, to bend light without losses and to localize light in periodic, multidimensional arrangements. More recently, non-radiative energy transfer between nanostructures attracted some interest for the design of subwavelength optical devices. The mapping of the electromagnetic field bound to such devices is important for the assessment of device functionality. As an example, Figure 10 shows the field distribution surrounding a chain of gold nanoparticles that was deposited atop a glass prism. The entire structure was illuminated in total internal reflection. A glass fiber tip was used to locally probe the electromagnetic field and to reveal that the field is localized near individual particles [81]. Further investigations demonstrated propagation of light along heterogeneous optical nanowaveguides for several microns as well as electromagnetic coupling between separated telecommunications channels [82].

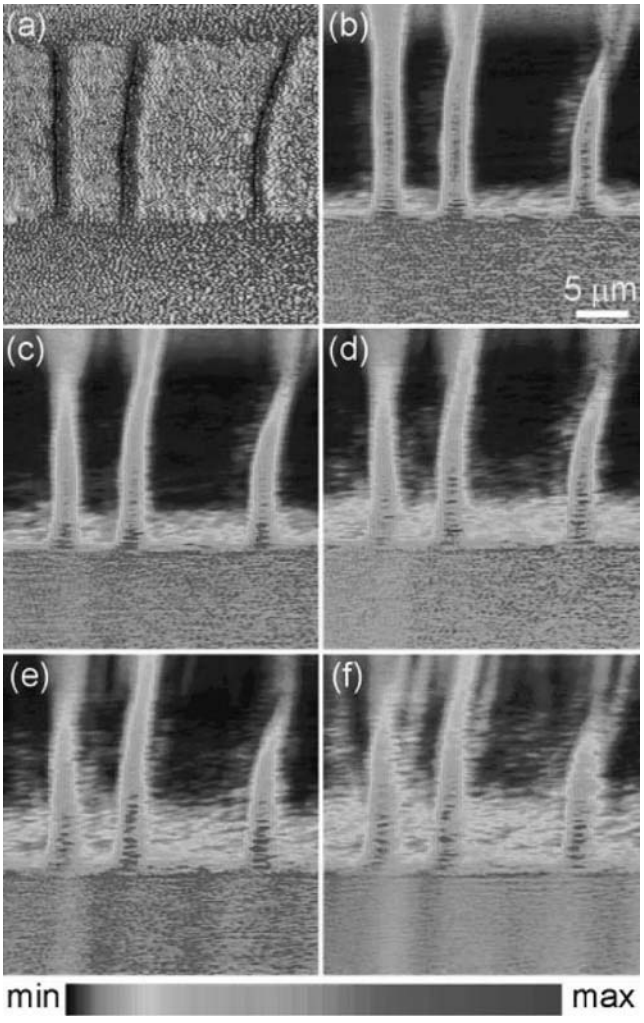

Figure 11. Surface plasmon guiding along Au nanochannels formed by surface corrugation. (a) Topographic image (30 μm by 30 μm) of the channels. (b–f) Surface plasmon intensity maps recorded with a glass fiber probe, excitation wavelengths: 713 nm, 750 nm, 785 nm, 815 nm, and 855 nm, respectively. From Ref. [83].

Near-field studies of metal structures supporting surface plasmons have shown that the plasmon field can be confined along a well-defined path such as line defect. Furthermore, the transmission of such a path can be influenced by varying the excitation wavelength. Figure 11 demonstrates this wavelength dependence for a series of gold channels [83]. In this experiment, a surface plasmon was excited by total internal reflection. By artificially corrugated the metal surface, plasmon propagation can be inhibited,

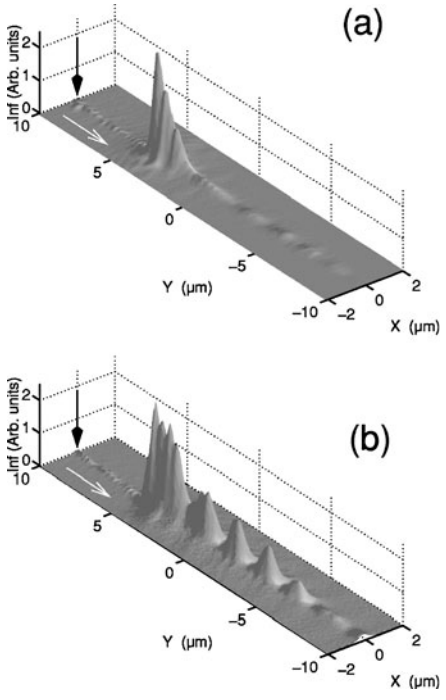

Figure 12. Field distribution along dielectric heterowires as measured with a glass tip. (a) Heterowire parameters do not allow the field to propagate. (b) The wire parameters have been changed and the field is transmitted for more than 10 μm. The black arrow shows the location of the micro-channel conducting the light to the heterowire. The white arrow represents the propagation direction. From Ref. [84].

and by leaving individual stripes uncorrugated plasmon waveguides are created. The surface plasmon wavelength was varied and its near-field intensity distribution was mapped out for each value of the wavelength. The image reveals important variations in the channel transmission as well as in the overall field distribution as the wavelength increases. Studies of this kind allow one to asses the propagation properties of surface plasmons for use as potential information lines between nanodevices.

Mesoscopic dielectric structures are another class of planar photonic crystals. An otherwise transparent reference medium is rendered opaque over some frequency range o by modulating its dielectric properties. Resonant optical tunneling can give rise to enhanced optical transfer through the medium, and near-field microscopy is an important tool for characterizing such enhanced transmission. An example is depicted in Figure 12, where two different heterowires composed of nanoscopic dielectric structures are excited in the same way. The wire in Fig. 12(a) does not support efficient propagation along the wire, whereas the wire in Fig. 12(b) exhibits enhanced transmission over 10 micrometers [84].

4.4. Nanolithography

Reducing the dimensions of structures and devices is one of the major achievements of nanotechnology. An example of the constant efforts in down-scaling is the famous Moore's law. In its 1965 prediction, G. Moore foresaw that the number of transistors on a silicon chip would increase by a factor two every second year. After nearly 40 years, Moore's vision still holds true today. However, optical projection lithography used to produce high-volume integrated circuits will soon reach its limit. It is anticipated that this technology will still be the workhorse through the 100 nm generation of devices, mainly influenced by the emergence of a new wavelength standard (193 nm). For features with smaller dimensions, a new generation of lithography will be required [85]. A variety of nanofabrication techniques have been investigated in the recent years as alternatives to classical optical projection lithography. Among them are nano-imprint lithography [86], micro-contact printing [87], electron beam [88], X-ray [89] and deep UV lithographies [90], atom manipulation [91], and finally near-field optical photolithography.

The pioneering work of Betzig and coworkers showed the feasibility of using localized fields created by a near-field probe to pattern a photoresist with sub-wavelength resolution [92]. The idea was further developed by Krausch [93] and Smolyaninov [94]. 100 nm size patterns, mostly composed of adjacent lines, were created on photoresist and subsequently transferred onto a substrate. It was pointed out that the light-sensitive polymer can also serve as a fingerprint for the field distribution near a the near-field probe. Davy *et al.* carried out a systematic study of this effect [95].

Most of near-field lithography studies use an optical fiber probe prepared as described in section 3.1. A line from an excimer or Argon laser is coupled to one end of the fiber. The fiber is held at a few nanometers from the photosensitive polymer surface to ensure that the evanescent components of the field interact with the substrate. The exposure time of the resist is usually controlled by an acousto-opto modulator. The resist is either developed to transfer the written patterns onto the substrate or analyzed directly after exposure. The analysis consists of measuring the physical photo-deformation of the surface by means of atomic force microscopy or shear-force microscopy.

The pattern size written with metal-coated fiber probes is so far limited between 60 to 100 nm. Lateral dimensions are influenced by (i) the diameter of the near-field probe plays and (ii) by the exposure time. The latter defines the aspect ratio of a given structure and careful investigations of the exposure dosage are necessary. Near-field optical lithography can be fully exploited only if the thickness of the resist is thin enough (comparable to exponential decay length of the evanescent waves) [96]. In turn, it seems that the aspect ratio of a feature is limited to 4:1. An example of a $\sim$100 nm width photoimprinted pattern is depicted in Figure 13.

Near-field photolithography can also be accomplished by use of a metal tip that locally enhances the electromagnetic field. Similar to some of experiments described in the section on fluorescence and Raman microscopy, a suitably polarized laser beam irradiates and excites electronic resonances that give rise to an enhanced field at the extremity of the tip. Studies have shown that the confinement of the field can be

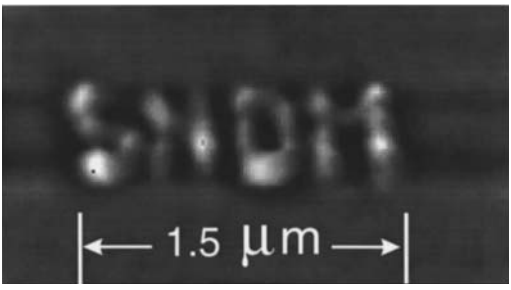

Figure 13. Photodeformation of a sensitive polymer by the proximity of near-field probe. The line widths are about 100 nm on the thinnest sections. From Ref. [95].

localized down to a few nanometers [97]. This confined field is then used to expose a photosensitive resist [98, 99]. In a related approach consists the field enhancement at a metal tip is combined with the nonlinear properties of photoresists. The probability to create a two-photon absorption process in a material scales with the field intensity squared. Therefore, by choosing appropriate pulse shape, energy, and duration, farfield sub-diffraction patterning is possible [100]. The combination of local field enhancement and nonlinear interactions is therefore very promising [101]. Preliminary results showed features with size $\lambda/10$ (see Figure 14.).

Near-field patterning has been employed in various kinds of materials and substrates. The enhanced field near a metal tip can be employed to pattern thin aluminum films or to ablate parts of it [102]. Laser-induced thermal oxidation through local heating of the metal film by the tip extremity triggers the formation of an aluminum oxide. This nano-oxidation procedure generates patterns that act as electrically insulating domains and can be used to design two-dimensional electrode patterns [103]. Another interesting class of material suitable for nanopatterning is self-assembled monolayers (SAMs). SAMs find important applications in interface science, where they are used for cellular or protein attachment. Photopatterning of SAMs opens the possibility to fabricate biomolecular structures. Well-defined chemical patterns were obtained with sizes as small as 25 nm indicating the potential use of near-field optics in nanoscale photo-chemical processes [104]. Another example where near-field optics is used to induce material modification is ferroelectric surfaces. Patterns that show 60 nm linewidths were produced using metal-coated optical fibers [105].

4.5. Semiconductors

The steady miniaturization and optimization of communication and information processing devices requires ever-smaller semiconductor structures. The more conventional top down approach involves machining of macroscopic samples down to nanometer sizes using, for example, electron beam lithography. In the bottom-up approach, nanostructures such as quantum dots are assembled to form larger assemblies. In both cases, the resulting properties of the semiconductor are dominated by quantum effects and

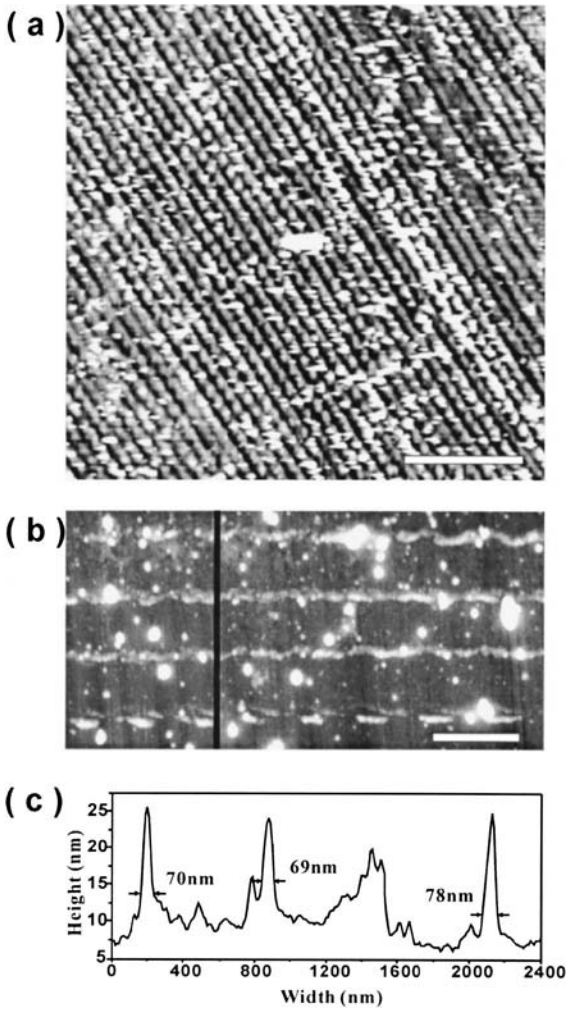

Figure 14. AFM images of two-photon produced line structures in SU-8 photoresist that was exposed by the enhanced field of metal coated silicon cantilever. The farfield peak intensities were (a) 0.9 TW/cm^2 and (b) 0.45 TW/cm^2. Panel (c) shows a cross sectional view (height profile) along the dark vertical line in (b), suggesting that two-photon apertureless near-field lithography can produce 72 nm ±10 nm features using 790 nm light. The scale bars in (a) and (b) are 5 and 1 μm, respectively. From Ref. [101].

can be essentially different from those of the bulk material. For example, electronic states of quantum dots are tuned through electron confinement. The development of new devices can benefit from the high-spatial confinement of light achieved in nano-optics. The method provides new insights into sample properties and can be used to identify, distinguish and address single quantum systems and to study coupling effects

of many quantum systems. The examples in this section illustrate the prospects and versatility of nano-optical methods in the field of semiconductor research.

Photoluminescence is an important tool for the study electronic of devices because it is nondestructive and nonintrusive. The optical and electronic properties of semiconductors are in fact intimately related: a quantum system exhibits quantized energy states that are identified by discrete emission wavelength. Near-field photoluminescence spectra provide a wealth of information on the spatial distribution of quantized features. In most investigations using near-field optics, charge carriers are photo-excited by the proximity of a near-field probe. Owing to the versatility of the technique, a probe is also able to locally detect sample luminescence. In the most advanced scheme, excitation and detection of photoluminescence is performed with the same near-field probe. This last scheme is usually employed for its relative simplicity of implementation in a cryogenic environment.

Near-field studies of a semiconductor system involve typically two kinds of physical measurements. In the first one, the excitation power is tuned to observe local band-filling phenomena. Spectral lines acquired at low excitation energy are characteristic of electron-hole recombinations of single exciton states whereas at higher powers biexcitons or multiexcitons are excited [106]. The second type of measurement is aimed at studying carrier diffusion by monitoring the spatial extent of the photoluminescence. This allows to assess the carrier confinement within a structure [107, 108]. An example of quasi one-dimensional excitons is depicted in Figure 15. The sample consists of a GaAs quantum wire clad between two AlGaAs barriers. Each wire segment is terminated by a quantum dot, which is characterized by a red-shifted emission from the quantum wire. The images represent a low-temperature photoluminescence map of the structure for different detection energies corresponding to peaks measured in farfield photoluminescence spectra. The spatial and spectral localization achieved by near-field microscopy permitted the assignment the emission energy to particular regions of the semiconductor structure.

The integration of devices made of different materials, *i.e.* heterostructures, is the key to modern electronics and optoelectronic technologies. Characterization of such structures is a major area of study in material science. Near-field techniques provide a means to locally address the electro-optical properties of ordered regions, domains, and dislocations [109, 110, 111, 112, 113]. Furthermore, the kinetic behavior of the carriers can be determined by locally exciting photocurrent. The photocurrent amplitude depends on the absorption length, the carrier diffusion constant, and carrier lifetime, whereas the spatial dependence is mainly governed by the diffusion length of the carriers [114, 115, 116].

Near-field techniques have also been successfully combined with time-resolved measurements to determine the dynamics of different photophysical processes. Time-resolved optical spectroscopy provides a wealth of information on the dynamic processes of free carriers and excitons. Real space transfer, trapping, dephasing, scattering and relaxation phenomena are of interest from the viewpoint of fundamental physics and device applications. The combination of femtosecond pump-probe spectroscopy and near-field optics provides direct insight into the spatio-temporal dynamic of

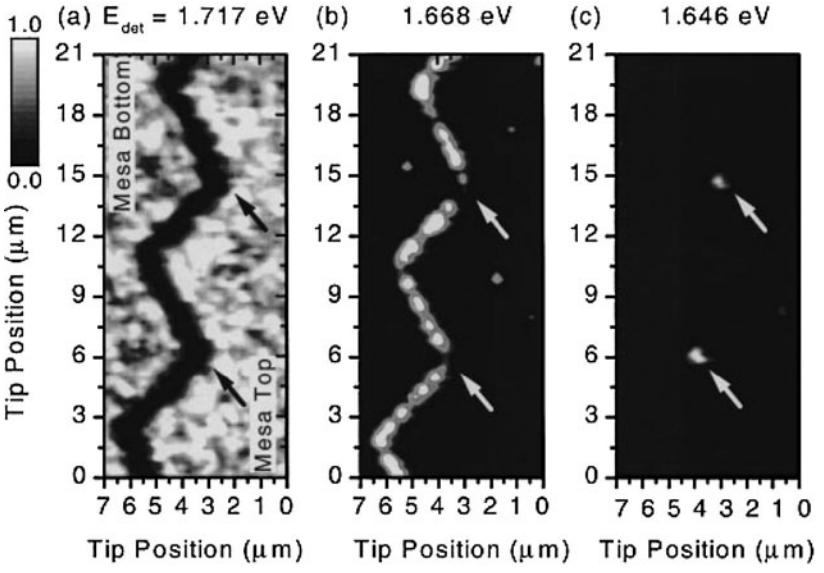

Figure 15. Low temperature (10 K) near-field images of the luminescence from a coupled quantum wire-quantum dot sample recorded at three different detection energies in an illumination/collection geometry. (a) quantum well emission, (b) quantum wire photoluminescence, and (c) quantum dot emission. From Ref. [108].

optical excitations in semiconductor structures. In these experiments, the pump and probe beam are usually provided by an ultrafast laser system. The carriers are photo-excited either in the farfield by the pump, and the change in absorption is measured locally [117, 118], or vise versa [119, 120]. Pump and probe can also be provided by the same aperture [121]. Without going into the details of these experiments, non-equilibrium carrier dynamics in low-dimension systems are investigated with good spatial (∼150 nm) and temporal resolution (∼200 fs).

5. PERSPECTIVES

Since the first experiment demonstrating sub-wavelength optical resolution, scanning near-field optical microscopy provided scientists with the possibility to access optical properties that were previously invisible. This unique capability triggered a rapid development of the technique and brought together scientists from various fields ranging from materials science to biology. Unfortunately, technical challenges are preventing near-field microscopy to be a routine characterization technique, as for example, atomic force microscopy. The main limiting factor remains the reliable fabrication of near-field probes. 20 years after the first realization, simple experimental factors such as the optimum tip geometry and tip material need still to be defined. Hopefully, recent advances in nanofabrication together with a better understanding of nanoscale optical

phenomena will permit to overcome this technical barrier. Despite its limitations, SNOM is used in various fields of sciences owing to its unique versatility. Depending on the specific configuration, a near-field signal can be sensitive to the local electric field, magnetic field, permittivity, chemical properties, or topography. The technique is at the origin of fascinating scientific discoveries in the emerging field of nanoscience. The instrument permitted breakthrough studies of individual molecules with unprecedented details (absorption moment orientation, lifetime and dynamical properties . . .), and opened the possibility to perform vibrational spectroscopy and chemical imaging with optical resolutions down to 10 nm. It also allowed for the first time a direct observation of surface plasmons and triggered advances in plasmonic and photonic devices. There is simply no other means to map an electromagnetic field distribution with nanoscale resolution. However, interesting questions are yet to be answered. How far can we push resolution? Are we already facing fundamental limits (material skin depth . . .) preventing? How will a near-field probe look like in 5 years? These questions will be answered in the coming years and the time ahead will generate new insight into nanoscale properties. In turns, near-field microscopy will be pushed from exploratory nanoscience to a commercial nanotechnology.

REFERENCES

[1] E. Abbe, *Archiv. f. Mikroscop*. 9 (1873) 413.
[2] Lord Rayleigh, *Phil. Mag*. 42 (1896) 167.
[3] E. H. Synge, *Phil. Mag*. 6 (1928) 356.
[4] D. W. Pohl, W. Denk and M. Lanz, *Appl. Phys. Lett*. 44 (1984) 651.
[5] A. Lewis, M. Isaacson, A. Murray and A. Harootunian, *Biophys. J*. 41 (1983) 405a.
[6] E. Betzig, P. L. Finn, and J. S. Weiner, *Appl. Phys. Lett*. 60 (1992) 2484.
[7] K. Karrai and D. R. Grober, *Appl. Phys. Lett*. 66 (1995) 1842.
[8] O. J. F. Martin, *J. Microscopy*. 194 (1999) 235.
[9] E. Betzig and J. K. Trautman, *Science* 257 (1992) 189.
[10] D. R. Turner, US-Patent, 4.469.554 (1983).
[11] P. Lambelet, A. Sayah, M. Pfeffer, C. Philipona, and F. Marquis-Weible, *Appl. Opt*. 37 (1998) 7289.
[12] R. Stöckle, Ch. Fokas, V. Deckert, R. Zenobi, B. Sick, B. Hecht and U.P. Wild, *Appl. Phys. Lett*. 75 (1999) 60.
[13] T. Saiki, S. Mononobe, M. Ohtsu, N. Saito and J. Kusano, *Appl. Phys. Lett*. 68 (1996) 2612.
[14] P. Hoffmann, B. Dutoit and R.-P. Salathé, *Ultramicroscopy* 61 (1995) 165.
[15] P. Moar, F. Ladouceur and L. Cahill, *Appl. Opt*. 39 (2000) 1966.
[16] L. Novotny, D. W. Pohl and B. Hecht, *Opt. Lett*. 20 (1995) 970.
[17] A. W. Snyder and J. D. Love, *Optical waveguide theory*, Chapman and Hall, 1983.
[18] L. Novotny and C. Hafner, *Phys. Rev. E*. 50 (1995) 4095.
[19] Th. Pagnot and Ch. Pierali, *Opt. Comm*. 132 (1996) 161.
[20] T. Saiki and K. Matsuda, *Appl. Phys. Lett*. 74 (1999) 2773.
[21] D. Mulin, D. Courjon, J.-P. Malugani and B. Gauthier-Manuel, *Appl. Phys. Lett*. 71 (1997) 437.
[22] A. Bouhelier, J. Toquant, H. Tamaru, H.-J. Güntherodt, D. W. Pohl and G. Schider, *Appl.Phys. Lett*. 79 (2001) 683.
[23] Th. Lacoste, Th. Huser, R. Prioli and H. Heinzelmann, *Ultramicroscopy* 71 (1998) 333.
[24] J. A. Veerman, A. M. Otter, L. Kuipers and N. F. Hulst, *Appl. Phys. Lett*. 72 (1998) 3115.
[25] A. Naber, D. molenda, U. C. Fischer, H.-J. Maas, C. Hüppener, N. Lu and H. Fuchs, *Phys. Rev. Lett*. 89 (2002) 210801.
[26] U. Ch. Fischer and M. Zapletal, *Ultramicroscopy* 42–44 (1992) 393.
[27] G. Schürmann, P. F. Indermühle, U. Staufer and N. F. de Rooij, *Surf. Inter. Anal*. 27 (1998) 299.

[28] H. Zhou, B. K. Chong, P. Stopford, G. Mills, A. Midha, L. Donaldson and J. M. R. Weaver, *J. Vac. Sci. Technol. B* 18 (2000) 3594.
[29] D. Haefliger and A. Stemmer, *Appl. Phys. Lett*. 80 (2002) 3397.
[30] R. Hillenbrand, and F. Keilmann, *Phys. Rev. Lett*. 85 (2000) 3029.
[31] J. Wessel, *J. Opt. Soc. Am. B* 2 (1985) 1538.
[32] H. G. Frey, F. Keilmann, A. Kriele and R. Guckenberger, *Appl. Phys. Lett*. 81 (2002) 5030.
[33] A. Bouhelier, J. Renger, M. R. Beversluis, and L. Novotny, *J. Microscopy* 210 (2003) 220.
[34] D. Courjon, K. Sarayeddine and M. Spajer, *Opt. Commun*. 71 (1989) 23.
[35] M. Vacha, S. Takei, K.-I. Hashizume, Y. Sakakibara and T. Tani, *Chem. Phys. Lett* 331 (2000) 387.
[36] For a review see W. E. Moerner and D. P, Fromm, *Rev. Sci. Instr.* 74 (2003) 3597.
[37] E. Betzig, A. Lewis, A. Harootunian, M. Isaacson and E. Kratschemer, *Biophys. J.* 49 (1986) 269.
[38] U. Fischer, *J. Opt. Soc. Am. B* 3 (1986) 1239.
[39] E. Betzig and R. Chichester, *Science* 262 (1993) 1422.
[40] R. X. Brain, R. C. Dunn, X. S. Xie and P. T. Leung, *Phys. Rev. Lett*. 75 (1995) 4771.
[41] W. Lukosz and R. E. Kunz, *J. Opt. Soc. Am*. 6 (1977) 1615.
[42] H. Gersen, M. F. Garcia-parajo, L. Novotny, A. Veerman L. Kuipers and N. F. van Hulst, *Phys. Rev. Lett*. 85 (2000) 5315.
[43] W. P. Ambrose, P. M . Goodwin, J. C. Martin and R. A. Keller, *Phys. Rev. Lett*. 72 (1994) 160.
[44] J. A. Veerman, M. F. Garcia-Parajo, L. Kuipers, and N. F. van Hulst, *Phys. Rev. Lett*. 83 (1999) 2155.
[45] C. Höppener, D. Molenda, H. Fuchs and A. Naber, *J. Microcoscopy* 210 (2003) 288.
[46] N. Hosaka and T. Saiki, *J. Microscopy* 202 (2000) 362.
[47] C. J. Bouwkamp, *Rep. Phys.* 5 (1950) 321.
[48] S. Nie and S. R. Emory, *Science* 275 (1997) 1102.
[49] E. J. Sanchez, L. Novotny and X. Xie, *Phy. Rev. Lett*. 82 (1999) 4014.
[50] T. Ha, Th. Enderle, D. F. Ogletree, D. S. Chemla, P. R. Selvin and S. Weiss, *Proc. Natl. Aca. Sci*. 93 (1996) 6264.
[51] G. T. Shubeita, S. K. Sekatsii, M. Chergui, M. Dietler and V. S. Letokhov, *Appl. Phys. Lett*. 74 (1999) 3453.
[52] S. A. Vickery and R. C. Dunn, *Biophysis. J.* 76 (1999) 1812.
[53] C. L. Jahncke, H. D. Hallen and M. A. Paesler, *J. Raman Spectrosc*. 27 (1996) 579.
[54] J. Prikulis, K. V. G. K. Murty, H. Olin and M. Käll, *J. Microscopy* 210 (2003) 269.
[55] P. G. Gucciardi, S. Trusso, C. Vasi, S. Patanè and M. Allegrini, *J. Microscopy* 209 (2003) 228.
[56] R. M. Stöckle, Y. D. Suh, V. Deckert and R. Zenobi, *Chem. Phys. Lett*. 318 (2000) 131.
[57] N. Hayazawa, Y. Inouye, Z. Sekkat and S. Kawata, *J. Chem. Phys*. 117 (2002) 1296.
[58] L. T. Nieman, G. M. Krampert and R. E. Martinez *Rev. Sci. Instrum*. 72 (2001) 1691.
[59] A. Hartschuh, E. J. Sánchez, X. S. Xie and L. Novotny, *Phys. Rev. Lett*. 90 (2003) 095503.
[60] M. S. Anderson, *Appl. Phys. Lett*. 76 (2000) 3130.
[61] B. Pettinger, G. Picardi, R. Schuster and G. Ertl, *Single Mol*. 5 (2002) 285.
[62] A. Hartschuh, N. Anderson and L. Novotny, *J. Microscopy* 210 (2003) 234.
[63] E. J. Ayars, H. D. Hallen and C. L. Jahncke, *Phys. Rev. Lett*. 85 (2000) 4180.
[64] J. T. Krug II, E. J. Sánchez and X. S. Xie, *J. Chem. Phys*. 116 (2002) 10895.
[65] S. Grésillon, L. Aigouy, A. C. Boccara, J. C. Rivoal, X. Quelin, C. Desmarest, P. Gadenne, V. A. Shubin, A. K. Sarychev and V. M. Shalaev, *Phys. Rev. Lett*. 80 (1999) 4520.
[66] M. I. Stokman, *Phys. Rev. Lett*. 84 (2000) 1011.
[67] H. Raether, *Excitation of Plasmons and Interband Transitions by Electrons*, Springer Tracts in Modern Physics Vol. 88, edited by G. Höhler, (Springer-Verlag, Berlin 1980).
[68] H. Raether, *Surface Plasmons*, Springer Tracts in Modern Physics Vol. 111, edited by G. Höhler, Springer-Verlag, Berlin (1988).
[69] For a review see W. L. Barnes, A. Dereux and T. W. Ebessen, *Nature* 424 (2003) 824.
[70] A. Otto, *Z. Angew. Phys*. 27 (1968) 207.
[71] E. Kretschmann and H. Raether, *Z. Naturforsch*. 23a (1968) 2135.
[72] H. Diltbacher, J. R. Krenn, N. Fleidj, B. Lamprecht, C. Schider, M. Salermo, A. Leitner and F. R. Aussenegg, *Appl. Phys. Lett*. 80 (2002) 404.
[73] B. Hecht, H. Bielefeldt, L. Novotny, Y. Inouye and D. W. Pohl, *Phys. Rev. Lett*. 77 (1996) 1889.
[74] P. Dawson, F. de Fornel and J.-P. Goudennet, *Phys. Rev. Lett* 72 (1994) 2927.
[75] I. I. Smolyaninov, D. L. Mazzoni, J. Mait and C. C. Davis, *Phys. Rev. B*. 56 (1997) 1601.
[76] A. Bouhelier, Th. Huser, H. Tamaru, H.-J. Güntherodt, D. W. Pohl, F. Baida and D. Van Labeke, *Phys. Rev. B*. 63 (2001) 155404.

[77] C. Sönnichsen, A. C. Duch, G. Steininger, M. Koch, G. von Plessen and J. Feldmann, *Appl. Phys. Lett.* 76 (2000) 140.
[78] B. Hecht, H. Bielefeldt, L. Novotny, Y. Inouye, and D. W. Pohl, *Phys. Rev. Lett.* 77 (1996) 1889.
[79] A. Bouhelier, T. Huser, J. M. Freyland, H. J. Güntherodt and D. W. Pohl, *J. Microscopy* 194 (1999) 571.
[80] B. Dragnea, J. M. Szarko, S. Kowarik, T. Weimann, J. Feldmann and S. R. Leone, *Nano Lett.* 3 (2003) 3.
[81] J. Krenn, A. Dereux, J. C. Weeber, E. Bourillot, Y. Lacroute, J. P. Goudonnet, G. Schider, W. Gotschy, A. Leitner, F. R. Aussenegg and C. Girard, *Phys. Rev. Lett.* 82 (1999) 2590.
[82] D. Mulin, M. Spajer, D. Courjon, F. Carcenac and Y. Chen, *J. Appl. Phys.* 87 (2000) 534.
[83] S. I. Bozhevolny, V. S. Volkov, K. Leosson and A. Boltasseva, *J. Microscopy* 209 (2003) 209.
[84] R. Quidant, J.-C. Weeber, A. Dereux, D. Peyrade, Ch. Girard and Y. Chen, *Phys. Rev. E* 62 (2002) 036616.
[85] For a review see for instance S. Wittekoek, *Microelectron. Eng.* 23 (1994) 43.
[86] S. Y. Chou, P. R. Krauss and P. J. Renstrom, *Science* 272 (1996) 85.
[87] A. Kumar and G. M. Whitesides, *Appl. Phys. Lett.* 63 (1993) 2002.
[88] P. Rai-Choudhury, *Handbook of Microlithography, and Microfabrication,* Spie Optical Engineering Press, 1994.
[89] J. R. Sheats and B. W. Smith *Microlithography Science & Technology*, (1988).
[90] M. D. Levenson, P. J. Silverman, R. George, S. Wittekoek, P. Ware, C. Sparkes, L. Thompson, P. Bischoff, A. Dickinson and J. Shamaly, *Solid State Technol.* 38 (1995) 81.
[91] D. M. Eigler and E. K. Schweizer, *Nature* 344 (1990) 524.
[92] E. Betzig, J. K. Trautman, T. D. Harris, J. S. Weiner and R. L. Kostelak, *Science* 251 (1991) 1468.
[93] G. Krausch, S. Wegscheider, A. Kirsch, H. Bielefeldt, J. C. Meiners and J. Mlynek, *Opt. Commun.* 119 (1995) 283.
[94] I. I. Smolyaninov, D. L. Mazzoni and Ch. C. Davis, *Appl. Phys. Lett.* 67 (1995) 3859.
[95] S. Davy and M. Spajer, *Appl. Phys. Lett.* 69 (1996) 3306.
[96] A. Naber, H. Kock and H. Fuchs, *Scanning* 18 (1996) 567.
[97] L. Novotny, R. X. Bian and X. Sunney Xie, *Phys. Rev. Lett.* 79 (1997) 645.
[98] F. H'dhili, R. Bachelot, G. Lerondel, D. Barchiesi and P. Royer, *Appl. Phys. Lett.* 79 (2001) 4019.
[99] A. Tarun, M. Rosendo, H. Daza, N. Hayazawa, Y. Inouye and S. Kawata, *Appl. Phys. Lett.* 80 (2002) 3400.
[100] S. Kawata, H. B. Sun, T. Tanaka and K. Takada, *Nature* 412, 697 (2001).
[101] X. Yin, N. Fang, X. Zhang, I. B. Martini and B. Schwartz, *Appl. Phys. Lett.* 81 (2002) 3663.
[102] S. Nolte, B. N. Chichkov, H. Welling, Y. Shani, K. Lieberman and H. Terkel, *Opt. Lett.* 24 (1999) 914.
[103] D. Haefliger and A. Stemmer, *Ultramicroscopy* 209 (2003) 150.
[104] S. Sun, K. S. L. Chong and G. J. Leggett, *J. Am. Chem. Soc.* 124 (2002) 2415.
[105] J. Massanell, N. Garcìa and A. Zlatkin, *Opt. Lett.* 21 (1996) 12.
[106] M. Brun, S. Huant, J. C. Woehl, J.-F. Motte, L. Marsal and H. Mariette, *J. Microscopy* 202 (2001) 202.
[107] Y. Toda, M. Kourogi, M. Ohtsu, Y. Nagamune and Y. Arakawa, *Appl. Phys. Lett.* 69 (1996) 827.
[108] F. Intonti, V. Emiliani, C. Lienau, T. Elsaesser, R. Noetzel and K. H. Ploog, *J. Microscopy* 202 (2001) 193.
[109] J. W. P. Hsu, E. A. Fitzgerald, Y. H. Xie and P. J. Silverman, *Appl. Phys. Lett.* 65 (1994) 344.
[110] H. F. Hess, E. Betzig, T. D. Harris, L. N. Pfeiffer and K. W. West, *Science* 264, 1740 (1994).
[111] M. J. Gregor, P. G. Blome, R. G. Ulbrich, P. Grossmann, S. Grosse, J. Feldmann, W. Stolz, E. O. Göbel, D. J. Arent, M. Bode, K. A. Bertness and J. M. Olson, *Appl. Phys. Lett.* 67 (1995) 3572.
[112] T. D. Harris, D. Gershoni, R. D. Grober, L. Pfeiffer, K. West and N. Chand, *Appl. Phys. Lett.* 68 (1996) 988.
[113] A. A. McDaniel, J. W. P. Hsu and A. M. Gabor, *Appl. Phys. Lett.* 70 (1997) 3555.
[114] S. K. Buratto, J. W. P. Hsu, E. Betzig, J. K. Trautman, R. B. Bylsma, C. C. Bahr and M. J. Cardillo, *Appl. Phys. Lett.* 65 (1994) 2654.
[115] M. S. Ünlü, B. B. Goldberg, W. D. Herzog, D. Sun and E. Towe, *Appl. Phys. Lett.* 67 (1995) 1862.
[116] T. Saiki, N. Saito, J. Kusano and M. Ohtsu, *Appl. Phys. Lett.* 69 (1996) 644.
[117] J. Levy, V. Nikitin, J. M. Kikkawa, A. Cohen, N. Samarth, R. Garcia and D. D. Awschalom, *Phys. Rev. Lett.* 76 (1996) 1948.

[118] B. A. Nechay, U. Siegner, F. Morier-Genoud, A. Schertel and U. Keller, *Appl. Phys. Lett*. 74 (1999) 61.
[119] Richter, *J. Microscopy* 194 (1999) 393.
[120] M. Achermann, B. A. Nechay, U. Siegner, A. Hartmann, D. Oberli, E. Kapon and U. Keller, *Appl. Phys. Lett*. 76 (2000) 2695.
[121] V. Emiliani, T. Guenther, C. Lienau, R. Nötzel and K. H. Ploog, *J. Microscopy* 202 (2000) 229.

http://www.springer.com/978-1-4020-8003-6

Handbook of Microscopy for Nanotechnology
Yao, N.; Wang, Z.L. (Eds.)
2005, XX, 731 p., Hardcover
ISBN: 978-1-4020-8003-6